Applied Physics Letters

Transparent conductor-embedding nanolens for Si solar cells

Cite as: Appl. Phys. Lett. **106**, 151904 (2015); https://doi.org/10.1063/1.4918610
Submitted: 29 December 2014 . Accepted: 08 April 2015 . Published Online: 14 April 2015

Joondong Kim, Melvin David Kumar, Ju-Hyung Yun, Hyeong-Ho Park, Eunsongyi Lee, Dong-wook Kim, Hyunyub Kim, Mingeon Kim, Junsin Yi, Hongsik Kim, and Chaehwan Jeong

Transparent conductor-embedding nanolens for Si solar cells

Joondong Kim,[1,a),b)] Melvin David Kumar,[1,b)] Ju-Hyung Yun,[1] Hyeong-Ho Park,[2] Eunsongyi Lee,[3] Dong-wook Kim,[3] Hyunyub Kim,[4] Mingeon Kim,[4] Junsin Yi,[4,a)] Hongsik Kim,[1] and Chaehwan Jeong[5,a)]
[1]*Department of Electrical Engineering, Incheon National University, Incheon 406772, South Korea*
[2]*Applied Device and Material Lab., Device Technology Division, Korea Advanced Nano Fab Center (KANC), Suwon 443270, South Korea*
[3]*Department of Physics, Ewha Womans University, Seoul 120750, South Korea*
[4]*College of Information and Communication Engineering, Sungkyunkwan University, Suwon 440746, South Korea*
[5]*Applied Optics and Energy Research Group, Korea Institute of Industrial Technology, Gwangju 500480, South Korea*

(Received 29 December 2014; accepted 8 April 2015; published online 14 April 2015)

We present a large-scale applicable nanolens-embedding solar cell. An electrically conductive and optically transparent indium-tin-oxide (ITO) thin film was coated on a Si substrate. After then, periodically patterned ITO nanodome-arrays were formed on the ITO film by using a nano-imprint method. This structure is effective to reduce the incident light reflection for broad wavelengths and also efficient to drive the incident photons into a light-absorbing Si substrate. There exist two electric fields. One is by a p/n junction and the other is by the light absorption into Si. We designed nanolens structures to overlap two electric fields and demonstrate highly improved solar cell performances of current and voltage values from a planar structure. © *2015 AIP Publishing LLC*.
[http://dx.doi.org/10.1063/1.4918610]

Photoelectric devices can convert electrical energy into light emission such as light-emitting diodes (LEDs), displays, and lightings. Different from these passive devices, a solar cell is the only photoelectric device to generate electrical energy from the light.

Generally, we can consider two aspects to realize efficient solar cells. Optically, the utilization of incident light should be maximized at a certain photon energy level. This approach directly affects the efficiency of photo-generated carriers.[1–6]

For an optically effective design, light-reflection at a solar cell surface holds fundamental effect. As the light-reflection decreases, solar cells can have more chances to absorb the incoming light into semiconductor materials. Moreover, the enhancement of light travelling length inside the light-active semiconductor layer is also a crucial factor, especially for thin film-type solar cells.

Electrical aspect controls the overall performance solar cell efficiency.[7] Optically perfect structures, bearing near-zero reflection, showed much lower efficiency than the anticipation.[8–11] The optical benefit is hardly appeared in the electrically improved solar cells. This is mainly caused by the crucial electrical loss during the photo-generated carrier collection.

Nanostructures have an enormous advantage to enlarge the surface area at a fixed volume,[10,12,13] which is a promising feature of nanoscale designs for solar cells. The enlarged surface spontaneously enhances the photon absorption in the light-active semiconductor layer. However, conventional etching-method in the semiconductor layer readily induces defects along to the surface, which tremendously induce the recombination loss for solar cells. The previous researches suggest fundamental approaches for nanostructured solar cells.[1–13] Meanwhile, we can observe the limit in solar cell efficiencies. Additionally, a fancy concept has difficulty in the nanoscale fabrications and large-size applications. To resolve the limit and difficulty, we conceived a scheme to separate the optical and electrical designs in the nanostructured solar cells.

- Realization of optical benefits into electrical improvements by implementation of periodically nanoscale patterns on a transparent conducting layer.
- A thin transparent conductor film as an anti-reflection coating layer and an auxiliary electrode.
- Large scale-applicable printing fabrication without an etching process in semiconductor layer.

In order to make a p/n junction, a 4-in. wafer (Czochralski grown p-type Si base) was performed to form an n-type emitter. During a thermal doping process, phosphoryl chloride ($POCl_3$) as a doping agent was flowed into a doping furnace at 800 °C. After then, an indium-tin-oxide (ITO) film was coated on a Si substrate by using a DC magnetron system. A DC power (3.70 W/cm^2) was supplied to a 4-in. ITO target (In_2O_2 containing 10 wt. % SnO_2) at a processing temperature of 300 °C.

Figure 1(a) presents the processes of ITO nanodome structures on a Si substrate. A thin ITO film (~80 nm) was directly coated on Si. After that a commercial nano-imprint method was applied to form nanolens-arrays. Hole-patterns were imprinted onto the ITO film-coated Si substrate. The second ITO coating was performed in an e-beam evaporator system for good step coverage on nanoscale patterns. A lift-off process removed hole-patterns and spontaneously remained the ITO structures onto the ITO film. A field

a)Authors to whom correspondence should be addressed. Electronic addresses: joonkim@incheon.ac.kr; junsin@skku.edu; and chjeong@kitech.re.kr.
b)J. Kim and M. D. Kumar equally contributed to this work.

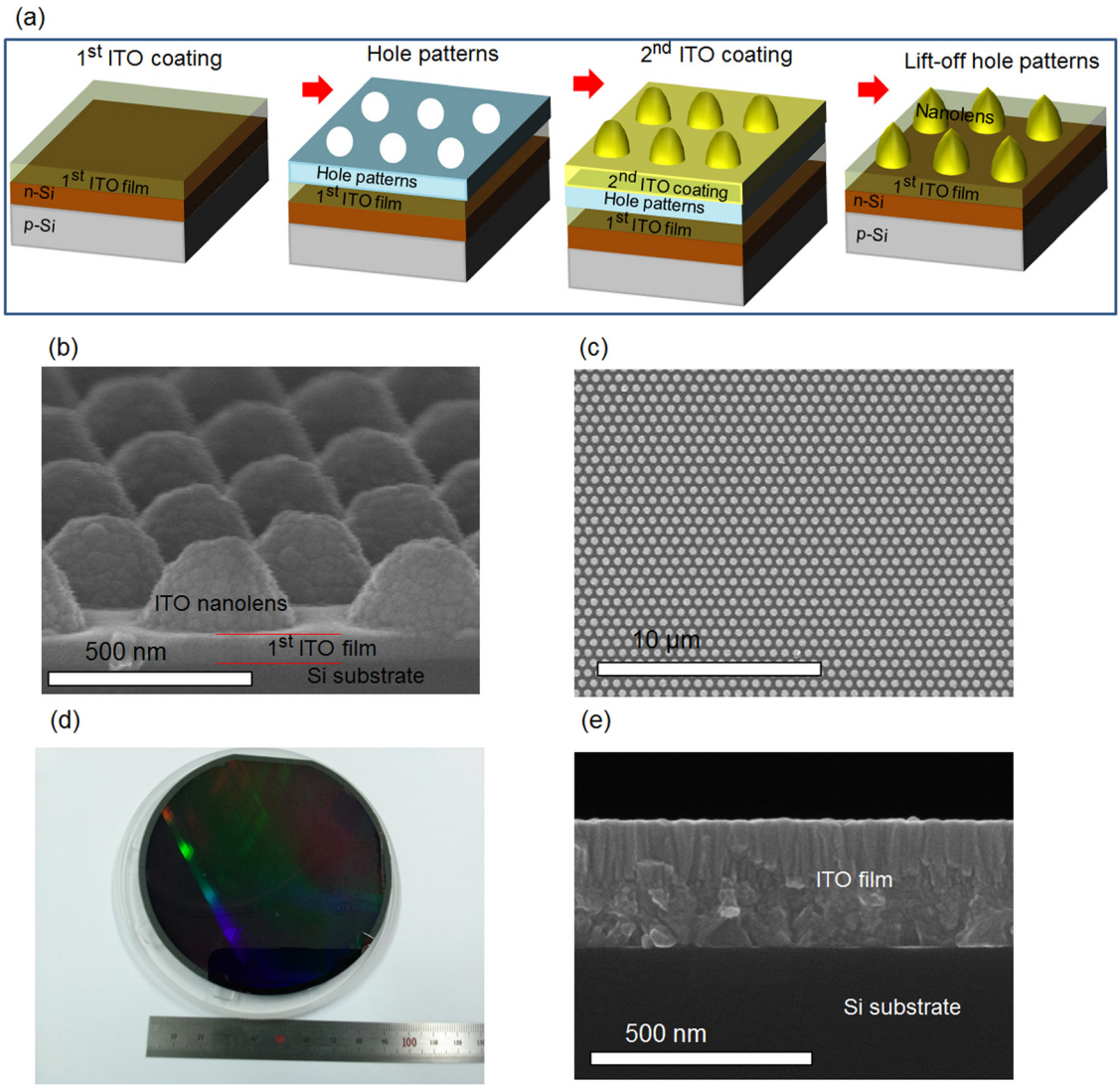

FIG. 1. (a) Fabrication steps of ITO nanolens structures on a Si substrate. (b) A cross-sectional view of an ITO nanolens. (c) A top-view of the formation of ITO nanolens-arrays. (d) A photo image of ITO nanolens patterned Si substrate. (e) A cross-sectional view of a flat 280 nm-ITO sample.

emission scanning electron microscope (FESEM, FEI sirion) was used to observe ITO structures.

Figure 1(b) shows a SEM image of ITO nanodome-sitting on an ITO film. The ITO film was previously formed to have about an 80 nm thickness before forming the ITO nanodome-arrays. A single nanodome has a height of 200 nm and a width of 380 nm. The nano-imprinted method is large scale available method to form uniform ITO nanolenses for a large area (Figure 1(c)). Figure 1(d) is a photo image of ITO nanodome patterns on a Si substrate. For a comparison, a single flat ITO film of 280 nm was prepared, as shown in Figure 1(e), for further investigations. Hereafter, a nanodome-sitting on an ITO film is referred as an ITO nanolens device and a single 280 nm-thick ITO film as a flat 280 nm-ITO device, respectively.

In order to analyze the optical performances of ITO structures, the reflectance profiles were obtained for the wavelength (λ) range of $300 \leq \lambda \leq 1100$ nm, as shown in Figure 2. For a bare Si, the averaged reflectance value (ARV) was measured to be 36.48%. An ITO film coated on a Si substrate was effective to reduce the reflectance due to the intermediate refractive index (n) value (1.9) of ITO that buffers the sudden changes occur at the boundary Si ($n = 3.9$) and air ($n = 1.0$). An 80 nm-thick ITO coated Si (80 nm-ITO) had 16.31% ARV. The thickness of ITO (80 nm) was determined by the quarter wavelength anti-reflection approach ($d = \lambda/4n$) method for a targeted wavelength ($\lambda = 600$ nm).[7]

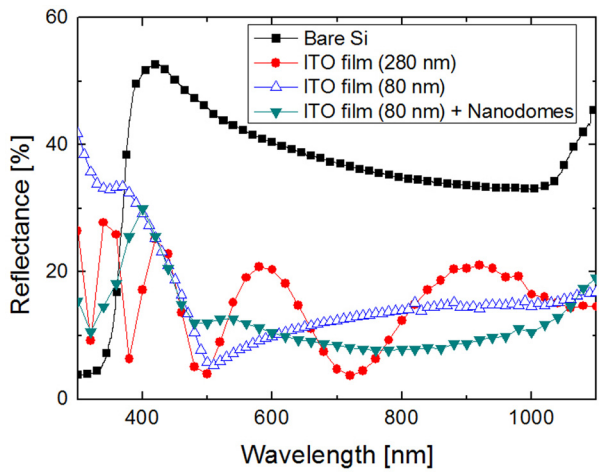

FIG. 2. Reflectance profiles.

TABLE I. Device performances.

	ITO film	ITO nanolens
Average reflectance (%)	14.94	12.4
Sheet resistance (Ω/□)	21	14
V_{oc} (mV)	527	584
J_{sc} (mA)	27.15	30.11
Efficiency (%)	10.9	13.5
Fill factor (%)	75.7	77.1
Series resistance (Ω)	0.210	0.168
Shunt resistance (Ω)	413.62	208.06

This is a main reason to employ the 80 nm-thick ITO film for a nanodome sample. We can clearly observe a significant ARV reduction by 12.40% from an ITO nanolens structure. In comparison, a 280 nm-ITO sample has an ARV of 14.94%. The ITO structures also serve as an electrical conductor. Table I presents the sheet resistance values of each ITO structure.

An emitter is a heavily doped n-type Si ($\sim 10^{20}/cm^3$), which form a p/n junction to a p-type Si ($\sim 10^{15}/cm^3$) substrate. Inside the p/n junction, major carriers of electrons in an n-Si emitter move to the p-Si base. Simultaneously, major carriers of holes in a p-Si move to n-Si side. These free-carriers transportation spontaneously induces depletion of moving carriers in a space charge region (SCR), remaining ions in a space charge region to establish a strong built-in electric field.

A doping level controls the SCR width on both the n-Si side (X_n) and the p-Si side (X_p). An SCR width of these doping levels was previously found to be 572 nm.[1] Most SCR is established into p-Si side, according to the following relation:

$$N_A(X_n) = N_D(X_P), \tag{1}$$

where N_A and N_D are doping concentration of p-Si and n-Si, respectively, as shown in Figure 3(a). The SCR has the higher collection efficiency of photo-generated carriers than those of neutral n-Si or p-Si region. Thus, it is known that an optimum location of SCR in geometry is crucial as well as critical to enhance solar cell performances.

The formation of a built-in potential (ϕ_{bi}) is deployed through the SCR, which is a barrier to control the current flows. Schematics of a nanolens device were presented in Figure 3(b). A photo image demonstrates the large size (3.2 × 3.2 cm^2) of the nanolens device (Figure 3(c)).

Solar cell devices were characterized for *I-V* curves, under a dark condition, as shown in Figure 4(a). For a forward bias, electrons in the n-Si readily move to the p-Si due to the lowering of ϕ_{bi}, whereas the motion of electrons is slowed down in the reverse bias due to the excessive barrier height. Bias controls the current flows resulting in the rectifying *I-V* profiles. All devices showed a clear rectifying current profile.

To measure the solar cell performances, two samples were electrically measured under one-sun illumination. A flat 280 nm-ITO Si sample provided an open circuit voltage (V_{oc}) of 527 mV with a short circuit current density (J_{sc}) of 27.15 mA/cm^2. For a nanolens device, we observed a significantly enhanced J_{sc} value (30.11 mA/cm^2), as shown in Figure 4(b) and Table I. In addition, V_{oc} value was much improved to be 584 mV. This current and voltage improvements from the nanolens solar cell can be attributed to the optical enhancement by the nanodome structure. As early mentioned, the nanodome surface evidently reduces the light reflection at the surface (Figure 2). Moreover, the shape of nanolens can tune the incident light into a Si.

We have measured internal quantum efficiency (IQE) profiles of the solar cells, as shown in Figure 4(c). The IQE of a photovoltaic device is mainly determined by the photo-generated carrier collection, excluding reflection effect. We clearly observed the improved IQE values for the wavelength above 550 nm. The wavelength region between 600 and 900 nm is the most substantial zone for Si based photovoltaics.[14,15] Generally, the light absorption of ITO layers increases at longer wavelength region due to their electronic transitions within a valence band and, consequently, it reduces the carrier collection efficiency.[16] However, the ITO nanolens structure effectively manages the long-wavelength photons.

In order to investigate the enhanced performances of ITO nanolens device, finite-difference time-domain (FDTD) calculations were performed to analyze the incident light

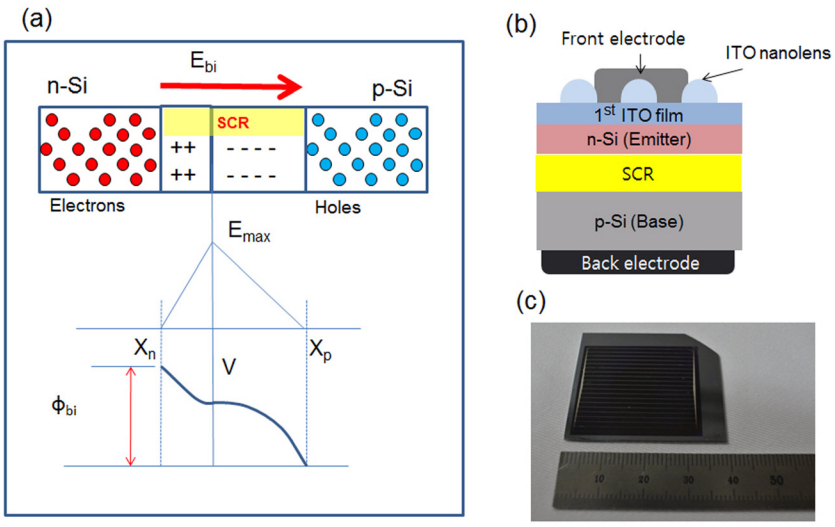

FIG. 3. (a) Schematics of p/n junction. Space charge region holds a strong electric field to give a built-in potential. Schematic representation of nanolens solar cell (b) and photo image (c).

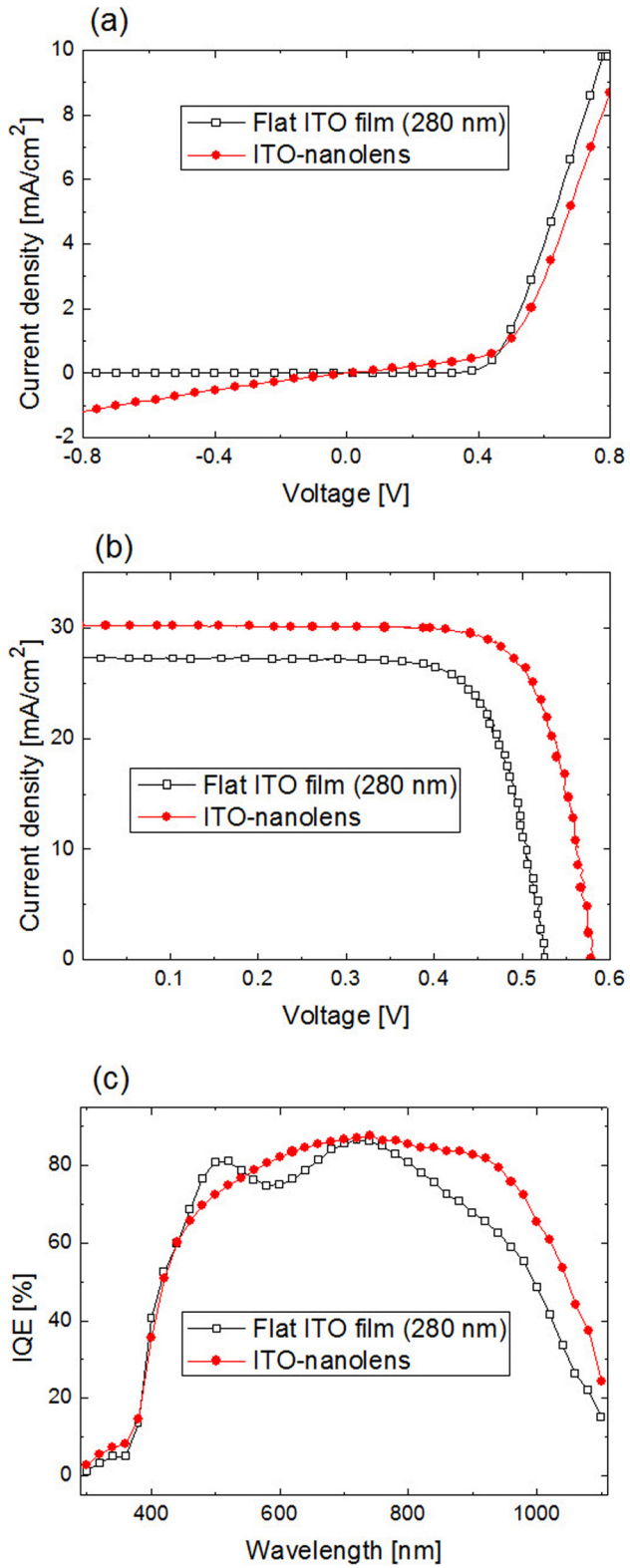

FIG. 4. (a) Dark *I-V* characteristics of a flat 280-ITO device and an ITO nanolens device. (b) One-sun illuminated *I-V* characteristics. (c) IQE profiles of solar cells.

propagation through the Si for a flat ITO device and a nanolens device.

For a short $\lambda = 420$ nm, the corresponding light is significantly scattered at a surface of the ITO nanolens. This phenomenon is related to the width of the nanolens (~380 nm), which is comparable to the wavelength. Although the scattering clearly exists at the surface, the incident light can be concentrated passing through the ITO nanolens, as shown in Figures 5(a) and 5(b). At the center of the nanolens (marked as "A line") strong electric field is induced, and hence, the field affects Si absorber. However, such strong light-induced electric field (E_{light}) is generated at shallow depths due to the large absorption coefficient of Si (α_{Si}).[17]

For larger wavelengths, α_{Si} values are moderate to extend the travelling length of incident light to longer depths. It is clearly observed that the ITO nanolens can efficiently prolong the light in deeper Si. A demonstration has been performed at $\lambda = 710$ nm, the normally incident light from the top of the nanolens is efficiently, typically, focused into a Si absorber. We can clearly observe the multiple peaks of light focuses. One strong peak (named as peak 1) was formed beneath the nanolens structure. Other peaks (peak 2 and peak 3) were spontaneously induced by light refraction by the neighboring nanolenses.

To investigate the wavelength-dependent light propagation, we have profiled the E_{light} in the Si absorber for the broad wavelengths (300–1100 nm), both for the ITO nanolens (Figure 5(c)) and the planar ITO structure (Figure 5(f)). A nanolens has a center position (A line), and thus the focusing effect of the ITO nanolens provides incident light-induced peak generation close to the SCR location. Since the focal length of the ITO nanolens in the Si absorber is extended by the larger Si refractive index, the peak positions approach the surface of the Si absorber at the longer wavelength. Around 450–750 nm, where the solar irradiance is relatively strong, the peak 1 is well positioned in the SCR. Meanwhile, the flat ITO film has no focusing effect and shows slightly increased E_{light} by increased λs. This is attributed to the lowering of α_{Si} values for longer λs.

Meanwhile, the flat ITO film has no focusing effect and shows slightly increased E_{light} by increased λs. This is attributed to the lowering of α_{Si} values for longer λs. The flat ITO structure merely forms plan wave propagation into Si without showing peak generation, as shown in Figure 5(f).

It suggests that the nanolens is appropriately designed and successfully modulates the broad λs to be focused into the SCR region, where exists the built-in electric field (E_{bi}) to bear the highest collection efficiency of the photo-generated carriers. Thus, the ITO nanolens device has a strong benefit to adjust the incident light to overlap E_{light} over E_{bi} to enhance the current value compared to that of the planar ITO device.

An ITO film with ITO nanolens-arrays are effective to reduce the electrical resistance and improve the light utilization in the light-absorbing materials, showing much improved current, voltage, and conversion efficiency. Although an identical nanodome shape was used, the solar cell performance is much affected by the location of an ITO film.[1] This may provide a useful design method for large area-applicable nanoscale patterned solar cells. We suggest that the position of an ITO film is very critical to realize the optical benefits to electrical enhanced performances. Further improvement may be realized by an optimum design of an opaque metal electrode,[7] control of thickness of transparent conductor film and species.[17–19]

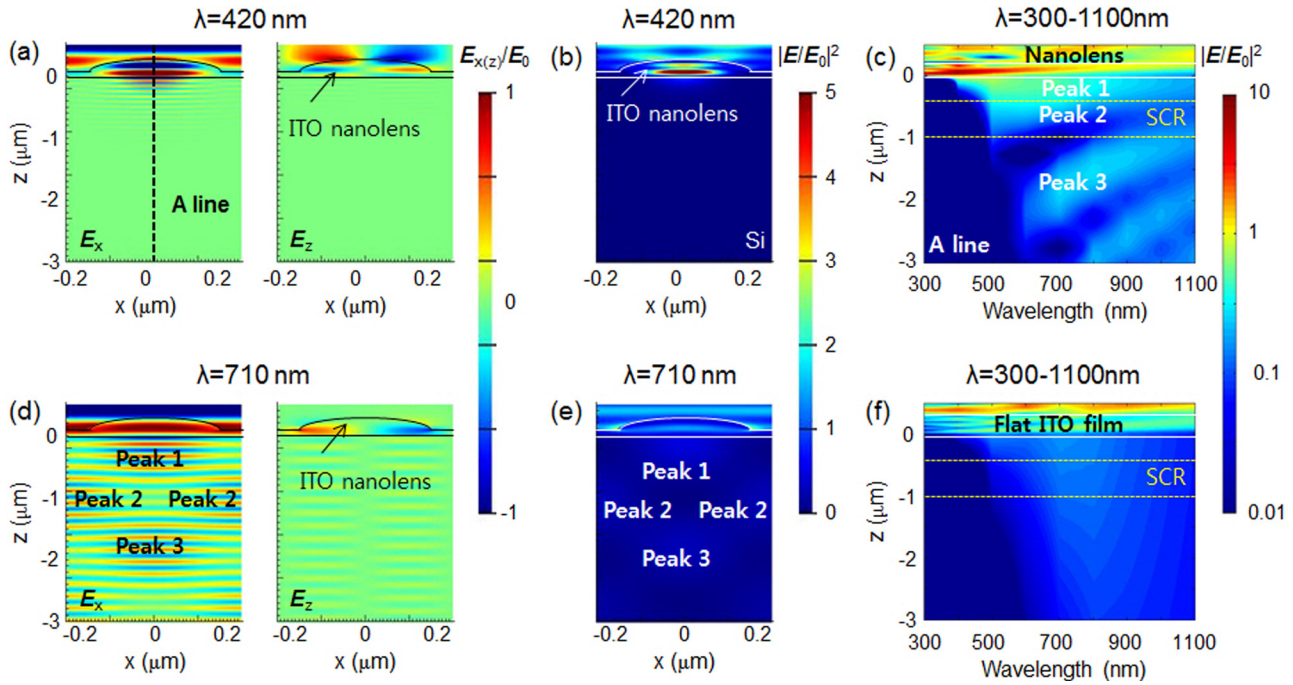

FIG. 5. Spatial electric field distribution in Si through a nanolens structure and a flat ITO film. Electric field distribution and electric field intensity at $\lambda = 420$ nm (a) and (b), and $\lambda = 710$ nm (d) and (e). Light-induced electric field distribution for broad wavelengths ($300 \leq \lambda \leq 1100$ nm) of (c) ITO nanolens structure and (f) flat ITO film.

In summary, a conceptual nanostructured solar cell has been demonstrated. Electrically conductive and optically transparent ITO materials were applied as the nanolens, which can focus the incident light into the light-active Si material. The bottom ITO film layer spontaneously provides an electrical connection to tie-up all single ITO nanolens sitting above it. The nanolens-arrays are remarkably effective to suppress the light reflection at a surface. Various lengths of wavelength lights can be focused into SCR through the nanolens geometries, and thus significantly enhanced electrical performances were achieved.

The authors acknowledge the financial support of the Korea Institute of Energy Technology Evaluation and Planning, in a grant funded by the Ministry of Knowledge and Economy (KETEP-20133030011000), and Business for Cooperative R&D between Industry, Academy, and Research Institute funded Korea Small and Medium Business Administration (C0219153). This work was also supported by post-doctoral research program through the Incheon National University (INU-2014). J. Yi and C. Jeong also note the support of KETEP-20143020010860.

[1]J. H. Yun, E. Lee, H. H. Park, D. W. Kim, W. A. Anderson, J. Kim, N. M. Litchinitser, J. Zeng, J. Yi, M. M. Kumar, and J. Sun, Sci. Rep. **4**, 6879 (2014).
[2]T.-G. Chen, P. Yu, S.-W. Chen, F.-Y. Chang, B.-Y. Huang, Y.-C. Cheng, J.-C. Hsiao, C.-K. Li, and Y.-R. Wu, Prog. Photovoltaics Res. Appl. **22**, 452 (2014).
[3]Y. Cho, M. Gwon, H. H. Park, J. Kim, and D. W. Kim, Nanoscale **6**(16), 9568 (2014).
[4]L. He, D. Lai, H. Wang, C. Jiang, and Rusli, Small **8**(11), 1664 (2012).
[5]S. Jeong, M. D. McGehee, and Y. Cui, Nat. Commun. **4**, 2950 (2013).
[6]A. Polman and H. A. Atwater, Nat. Mater. **11**, 174 (2012).
[7]M. Kim, J. Kim, H. Kim, J. Choi, J. Park, M. C. Ahn, and J. Yi, Curr. Appl. Phys. **13**, 808 (2013).
[8]P. Krogstrup, H. I. Jørgensen, M. Heiss, O. Demichel, J. V. Holm, M. Aagesen, J. Nygard, and A. Fontcuberta i Morral, Nat. Photonics **7**, 306 (2013).
[9]E. Lee, Y. Kim, M. Gwon, D.-W. Kim, S.-H. Baek, and J. Hyun Kim, Sol. Energy Mater. Sol. Cells **103**, 93 (2012).
[10]A. Mavrokefalos, S. E. Han, S. Yerci, M. S. Branham, and G. Chen, Nano Lett. **12**, 2792 (2012).
[11]S. Perraud, S. Poncet, S. Noël, M. Levis, P. Faucherand, E. Rouvière, P. Thony, C. Jaussaud, and R. Delsol, Sol. Energy Mater. Sol. Cells **93**, 1568 (2009).
[12]H. D. Um, K. T. Park, J. Y. Jung, X. Li, K. Zhou, S. W. Jee, and J. H. Lee, Nanoscale **6**, 5193 (2014).
[13]M. M. Adachi, M. P. Anantram, and K. S. Karim, Sci. Rep. **3**, 1546 (2013).
[14]N. Guo, J. Wei, Q. Shu, Y. Jia, S. Song, Y. Xu, H. Wang, P. Li, H. Zhu, K. Wang, and D. Wu, Appl. Phys A **107**, 911 (2012).
[15]S. E. Han and G. Chen, Nano Lett. **10**, 1012 (2010).
[16]D. R. Kim, C. H. Lee, P. M. Rao, I. S. Cho, and X. Zheng, Nano Lett. **11**, 2704 (2011).
[17]J. G. Kim and J. Kim, Sens. Actuators, A **217**, 183 (2014).
[18]J.-H. Yun, J. Kim, and Y. C. Park, J. Appl. Phys. **116**, 064904 (2014).
[19]M. M. D. Kumar, S. M. Baek, and J. Kim, Mater. Lett. **137**, 132 (2014).